

# Numerical Weather Prediction for the Bulgarian Antarctic Base Area and Sensitivity to the SST Variable



Boriana Chtirkova , Elisaveta Peneva , and Gergana Georgieva 

**Abstract** The weather forecast of good quality is essential for the humans living and operating in the Bulgarian Antarctic base (BAB), located on the Livingston Island coast at 62.64° S and 60.36° W. The numerical weather prediction models in southern high latitude regions still need improvement as the user community is limited, little test cases are documented and validation data are scarce. In this study, we suggest several ways to improve the local weather forecast model skill by modifications of the land cover and ocean temperature. We tested the sensitivity of the numerical weather prediction modelling system based on the Weather Research and Forecasting (WRF) model, configured for the BAB area, to the Sea surface temperature (SST) of the ocean around the island. The model configuration is described and details on the model performance are given. Several experiments with SST coming from different sources are performed, as well as experiments where the SST is scaled linearly. The conducted sensitivity experiments show that all of the considered meteorological variables are affected by the sea surface temperature, the most prominent differences being observed in the 2 m temperature field. With a uniform rise in SST, the corresponding tendencies are: an increase of the 2 m temperature, a decrease of the sea level pressure and an increase of the average wind speed. For the BAB region, the best results with unmodified SST data are obtained when using SST from the Copernicus Marine Service ocean model.

**Keywords** Numerical weather prediction · Antarctica · Sea surface temperature

## 1 Introduction

The Bulgarian Antarctic base “St. Kliment Ohridski” (BAB) is a national scientific facility, located on the coast of Livingston Island, South Shetland Islands, at 12–15 m above sea level. An average of 25 people work there during the austral summer,

---

B. Chtirkova (✉) · E. Peneva · G. Georgieva  
Department of Meteorology and Geophysics, Faculty of Physics, Sofia University “St. Kliment Ohridski”, 5 James Bourchier Blvd., 1164 Sofia, Bulgaria  
e-mail: [bshtirkova@uni-sofia.bg](mailto:bshtirkova@uni-sofia.bg)

© The Author(s), under exclusive license to Springer Nature Switzerland AG 2021  
N. Dobrinkova and G. Gadzhev (eds.), *Environmental Protection and Disaster Risks, Studies in Systems, Decision and Control* 361,  
[https://doi.org/10.1007/978-3-030-70190-1\\_23](https://doi.org/10.1007/978-3-030-70190-1_23)

339

usually from late November until early March. The weather in the region is mostly influenced by extratropical cyclones, which move west to east and tend to diffuse over land, due to friction. Thus, the weather is highly variable with intense storms and strong wind events occurring regularly.

Weather forecast of good quality is essential for the activities in BAB. A modelling system for weather prediction with high resolution in the BAB area based on the Weather Research and Forecasting (WRF) model is developed and validated in [2, 4]. The purpose of this work is to seek ways to improve prediction skill of this modeling system that could be implemented in operational mode. We have performed sensitivity experiments towards the land cover and the Sea Surface Temperature (SST) input variable and analyzed the obtained results.

The impact of SST on the weather forecast is more peculiar than that of land, because the SST is not only influenced by the heat fluxes between the atmosphere and ocean, but also by various fluxes and mixing processes in between ocean layers. Numerical modeling of the processes of interaction between the sea surface and the planetary boundary layer (PBL) have been a long term object of study. Tuleya and Kurihara [12] investigate the SST impact on the formation of tropical cyclones and demonstrate that increasing the SST with 4 K may result in a lower surface pressure by 7.6 hPa, compared to the case without altering the SST. While studying the effect of SST on the characteristics of Mediterranean cyclones with WRF, Miglietta et al. [8] reach the conclusions that increasing the SST leads to the following effects: deepening of the pressure minimum (as in [12]); the maximum wind speed at 10 m increases quasilinearly with SST; the maximum accumulated precipitation increases linearly with SST.

Senatore et al. [10] conduct a study with different SST datasets for the Mediterranean sea with WRF. Their conclusions show that the use of different datasets in long-term simulations leads to the same results, but the simulations of specific events are distinguished as a result of the SST representation.

On the basis of WRF simulations in the Yellow Sea and Eastern Chinese Sea regions, Bai et al. [1] demonstrate that the SST front is closely connected to the regulation of the marine atmospheric boundary layer (MABL). According to them, the various wind directions activate different MABL regulation mechanisms.

## 2 Model Configuration and Validation

The modelling system is based on the Weather Research and Forecasting model, version 4.0, developed by the National Center for Atmospheric Research (NCAR) and the National Centers for Environmental Prediction (NCEP). The numerical model uses a staggered Arakawa C-grid [11] and the nesting is performed in a ratio 9:3:1 km. The domain configuration is shown in Fig. 1: it is centered over BAB with coordinates  $62.64^\circ$  S and  $60.36^\circ$  W and consists of three nested domains d01, d02 and d03. The grid configuration is achieved using a Lambert conformal conic projection with standard parallels at  $60^\circ$  S and  $30^\circ$  S. The outermost domain—d01, with a resolution

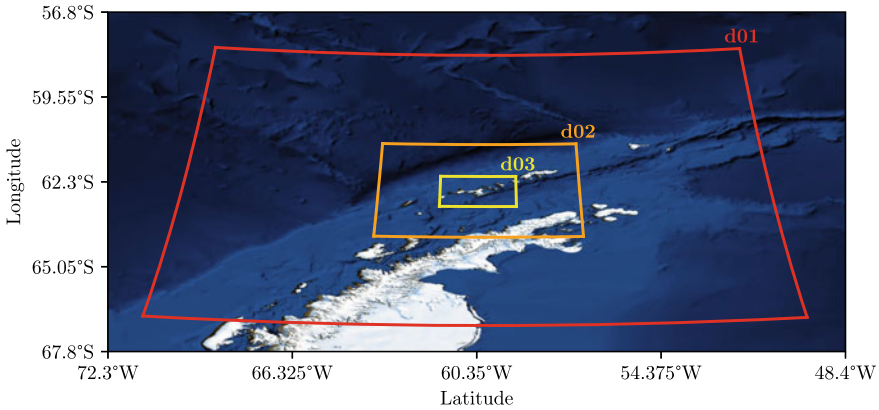


**Fig. 1** Three domains coverage—d01, d02 and d03. Background image from NASA Visible Earth—Blue Marble

of 9 km, has horizontal dimensions of 999 km in both directions and covers the northern part of the Antarctic Peninsula. It is a parent domain to the first nested domain—d02, with a horizontal resolution of 3 km and dimensions of 342 km in both directions. The finest domain—d03, nested in d02, has a horizontal resolution of 1 km, and covers the area of Livingston Island and its neighbouring small islands; the horizontal dimensions of d03 are 129 km in west–east direction and 111 km in south–north direction. The domain configuration is made so that there are no high mountains or complex relief near the domain borders.

### 2.1 Topography and Land Use Data

The land surface boundary condition of the modelling area is assembled via the WRF Preprocessing system program—*geogrid*, which interpolates topography and land use type data into the model grid. The topography data is taken from the GMTED2010 dataset, developed by the United States Geological Survey (USGS) and the National Geospatial-Intelligence Agency (NGA) and has a horizontal resolution of 225 m. The fitted in the finest domain topography is shown in Fig. 2a. A comparison with regional maps such as the map from [7] show that this dataset does not represent accurately Livingston Island. The mountain range Tangra mountains, reaching heights up to 1700 m, is represented as a flat surface with elevation of 50 m. Figure 2-a represents the topography grid in the finest domain, which has a number of points in the  $x$ -direction  $i_{max} = 129$  and in the  $y$ -direction— $j_{max} = 111$ , each grid point covers an area of  $1 \text{ km}^2$ .

The WRF model can perform mainly with two land use datasets, which cover the entire globe—USGS and MODIS. The USGS data is based on satellite advanced very-high-resolution radiometer (AVHRR) data, collected in the period April 1992–

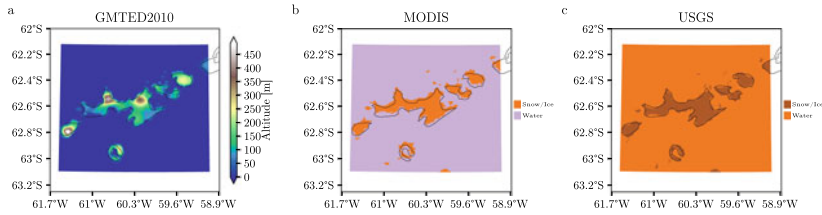


**Fig. 2** Topography (a) and land use type data from MODIS (b) and USGS (c) of the finest domain—d03 with a resolution of 1 km,  $i_{max} = 129$ ,  $j_{max} = 111$ . The coastlines on the image are taken from the Natural Earth Database (<https://www.naturalearthdata.com/>) and have a horizontal resolution of 10 m

March 1993. They contain 24 land use types and have a resolution of 1 km. The MODIS data (Moderate resolution imaging spectroradiometer) are gathered by NASA satellite missions in the period 2001–2005. They are made up of 20 land use type categories and their resolution reaches 500 m. A visual comparison between the MODIS and USGS land use type data is given in Figure 2b and c. According to both datasets, the entire domain area is described with only 2 land use types—snow/ice and water. The land use type is presented in numerical modelling through the following parameters: albedo  $\alpha$  (%), soil moisture availability  $M$  (%), surface emissivity,  $\epsilon$  (%), roughness length  $z_0$  (m), thermal inertia  $\lambda_T$  ( $\text{J m}^{-2} \text{K}^{-1} \text{s}^{-1/2}$ ) and surface heat capacity  $C$  ( $\text{J m}^{-2} \text{K}^{-1}$ ). The values of these parameters differ throughout the seasons and are used to describe the energy, momentum, water and heat fluxes. They slightly differ between the two datasets, mainly in the parameters  $z_0$  and  $\lambda_T$ , which are slightly higher within the MODIS data, but this distinction should not result in large computational differences. Comparing Fig. 2b and c, one can conclude that the coastal line, formed by the USGS data is not as continuous as the MODIS one. There is a slight displacement of the grid between the two datasets but this problem is eliminated with a manual choice of grid point to represent BAB. Having taken this into account, and the fact the MODIS data is more recently collected, the authors conclude it is better suited for the modelling system. However, the description of the whole Livingston Island as covered with snow and ice may not still be accurate in the recent years. Experiments from [4] demonstrate that using a different land use type with a lower heat capacity and a lower surface albedo, significantly improves the 2 m temperature forecast.

For a vertical coordinate in WRF, version 4.0, one can choose a terrain following (TF) coordinate or a hybrid vertical coordinate (HVC). In the present study, hybrid  $\eta$ -levels are used, unevenly distributed from the surface up to isobaric level 50 hPa. In order to determine the optimal number a vertical levels, a sample model run of a 72 h forecast with a different number of levels has been performed. All WRF experiments in the present study are run on the Sofia University Parallel Computer Center cluster PHYSON.<sup>1</sup> Three different vertical level configurations have been tested—with 35 vertical levels (close to the WRF minimum number), 50 and 70 levels. The  $\eta$ -levels

<sup>1</sup>PHYSON computer cluster: <http://physon.phys.uni-sofia.bg>.

from the three configurations are distributed with equal density near the surface but their distribution difference manifests after certain height. Hence, the description of the atmospheric state near the surface is similar, but the configuration with the least densely distributed levels in height fails to represent adequately high altitude phenomena, such as the polar jet stream. All simulations are performed using the same number of computer cores, 88 in this case, on the PHYSON cluster. For an optimal configuration, performed for a minimal time, the 50  $\eta$ -levels configuration is chosen.

## 2.2 *Model Parameterization Schemes*

Even though the high horizontal and vertical resolution of recent numerical models allows us to describe smaller scale phenomena, other physical processes on scales smaller than the model grid still need to be parametrized. The parametrization schemes and their combinations has a profound effect on numerical forecasting, especially in larger time scales and therefore the schemes should be chosen carefully. The subgrid processes that are or may be parametrized in WRF comprise of microphysics, convection, turbulence in the planetary boundary layer (PBL), interactions between the atmosphere and the surface layer and the longwave and shortwave radiation. The choice of parametrization schemes for the present study has been made through a literature review. The Antarctic Mesoscale Prediction System (AMPS) produces numerical forecasts for the Antarctic region, made through a modified PolarWRF [9]. The physics parametrization in the present configuration are chosen to be coherent and done in accordance with AMPS. The following schemes are used:

- Boundary layer: Mellor-Yamada-Janjic (Eta) TKE scheme
- Surface layer: Monin-Obukhov (Janjic Eta) scheme
- Land-surface interactions: Unified Noah Land Surface Model
- Microphysics: WSM 5-class scheme
- Long-wave radiation: RRTMG longwave radiation scheme
- Short-wave radiation: Goddard shortwave radiation scheme
- Convection: Kain-Fritsch (new Eta).

For a more detailed description of each scheme, the reader is referred to [11] or [3]. The Kain-Fritsch convection parametrization scheme is not used in the finest domain, because its horizontal resolution of 1 km can resolve convective processes.

The regional models need suitable atmospheric initial and lateral boundary conditions. They are taken from the GFS 0.25 Degree Historical Archive (NCEP, NWS, NOAA, U.S. 2015) and the lateral boundary conditions are updated every 3 h of the simulation. The sea surface temperature is also taken as a time varying surface boundary condition and is updated every 3 h into the simulation. The GFS model analysis in 0 UTC is taken as an initial condition for each of the three domains, while the lateral boundary conditions are given only to the outermost domain. Two-way nesting is performed, which means that the forecast in the parent domains is affected by the solutions in the finer domains.

### 2.3 Model Validation

The above described modelling system is validated in [4]. The authors consider three test cases with rapidly changing weather in the recent years records from the GFS model analysis and in-situ observations at BAB: 16–19 December 2016, 26 February–1 March 2020 and 25–28 January 2020. Each simulation is run over 3 days, starting at 0 UTC. The starting date is chosen so that the rapid change of weather happens at least 24h into the forecast. The model configuration has been validated against measurements from an automatic meteorological station at BAB, synoptic measurements in the nearby meteorological stations<sup>2</sup> and ERA-5 climatic hourly reanalysis data [6]. The in-situ measurements come from an automatic meteorological station Davis Vantage Vue for the 2016 and 2017 test cases, and an automatic station assembled by MeteoRocks<sup>3</sup> for the 2020 test case. The validated meteorological variables are temperature at 2 m, surface pressure, wind speed and wind direction. The total number of synoptic stations in the largest domain is 18, two of which lie in the finest domain. The synoptic observations from “Base Arturo Prat” with WMO index 89057 and coordinates 62.3° N, −59.41° E, are used in the comparison as indicative of the weather pattern in the region. They are in agreement with the observations from BAB in all test cases.

## 3 SST Sensitivity Experiments Planning

The results from the model validation in [4] show a general negative bias of the 2m temperature at BAB. Although in situ observations of that kind tend to increase the temperature around noon, the forecasted temperature curve is entirely below the observed one, even in the experiment with the lower thermal capacity of the land surface. One of the possible reasons for this could be the unrealistic representation of the Sea Surface Temperature, as the BAB is located on the beach. This was the motivation to test different sources of data for SST as model input. The default configuration of WRF model sets SST as initial condition which is not modified during the integration. We have tested the varying SST by activating the key *sst\_update* = 1. An alternative to the GFS SST variable is to use the data from the operational global ocean model of Copernicus Marine Environment Monitoring Service (CMEMS [5]). The hourly data are distributed in a grid with resolution 1/12 degree.

Comparing SST data between the GFS and the CMEMS operational ocean model for the three test cases, one can find significant differences between the two SST fields, together with different tendencies for the fields’ evolutions in time. Figure 3 demonstrates the difference in SST fields from the two models. The coldest areas of the ocean surface, reaching temperatures under 1 °C are shown by the GFS to be near the icy land areas. The CMEMS data show a significant temperature gradient,

---

<sup>2</sup>Ogimet: <https://www.ogimet.com>.

<sup>3</sup>The MeteoRocks project: <https://meteo.rocks/page/aboutus>.

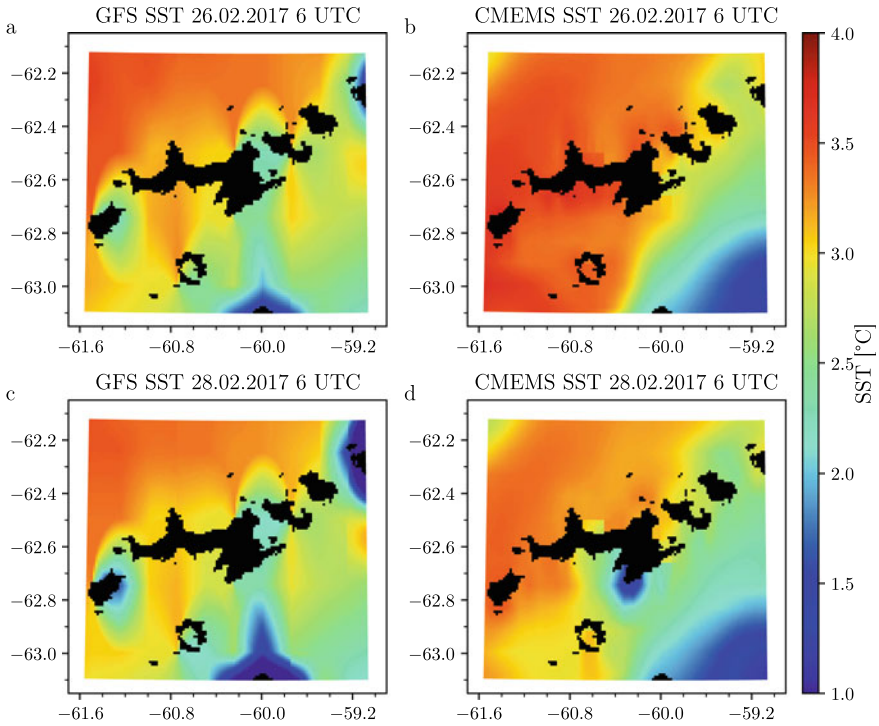


**Fig. 3** SST comparison between GFS and CMEMS data for 6 UTC on 26.02.2017 (a, b) and 6 UTC on 28.02.2017 (c, d).

orientated northwest-southeast, the cold part of which is propagating northwards like a front. The difference in time between Fig. 3a, b and c, d is 48 h, during which SST in the BAB bay has dropped less than 0.5 °C according to GFS and more than 1.5 °C as shown by CMEMS.

Another drastic difference between the two datasets from the 2020 test case can be seen in Fig. 4. In this case, the difference between the area average values of the two fields is larger—more than 2.5 °C. The tendencies of the two models, however, are similar to those in Fig. 3. The GFS model shows generally lower SSTs, which again do not change considerably in time, while the CMEMS model shows higher temperatures, which fall drastically with the cold front passage in both cases. The SST in the BAB bay has fallen by ~1.5 °C, while the SST around Rozhen peninsula (the southernmost part of Livingston island) has dropped by more than 2.5 °C, as seen in Fig. 4. The comparison between SST and sea water temperature at 3 m depth at the points shown in Fig. 4, can be made through the assumption of well-mixed water near the coast. The observed values at 3 m depth are closer to the temperatures, modeled by CMEMS. The in situ measurements also acknowledge the drop in temperature, caused by the front—the water temperature in the northern of the two points has fallen from 2.9 to 2.4 °C in two days.

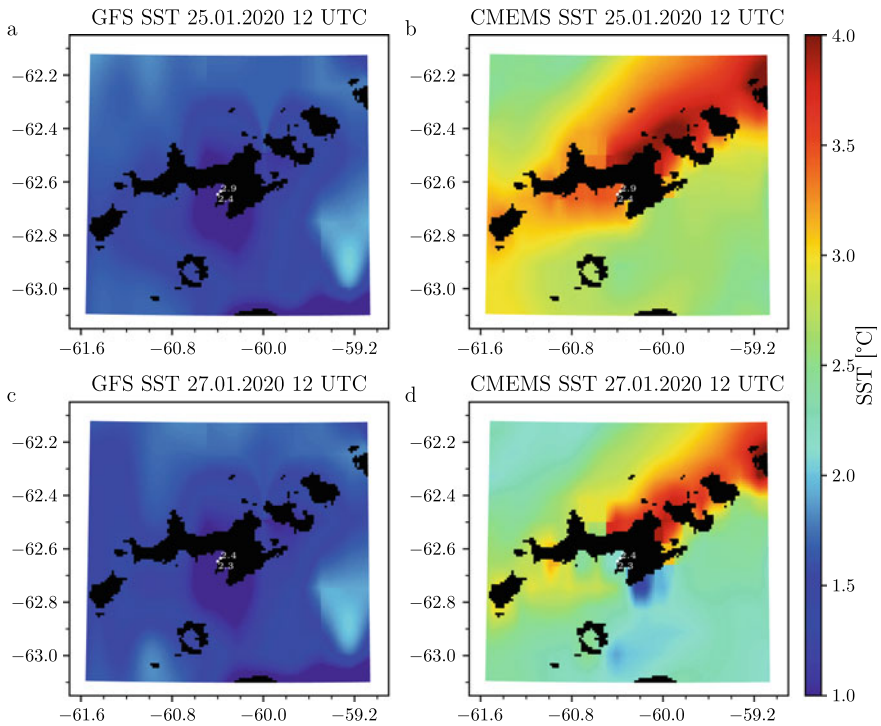


**Fig. 4** SST comparison between GFS and CMEMS data for 12 UTC on 25.01.2020 (**a, b**) and 12 UTC on 27.01.2020 (**c, d**). The white dots and the numbers beside them represent the water temperature at 3 m depth in °C for the corresponding day from in situ measurements at the dots' locations

By default, the WRF SST does not vary in time but remains constant throughout the length of the simulation, unless set up otherwise and provided suitable periodic boundary conditions. After the analysis of the two model fields, and taking into consideration previous numerical experiments, the following simulations are planned: numerical forecast with GFS SST data, where (1) SST does not vary in time; (2) SST varies in time; SSTs vary in time and their value at each point is (3) reduced by 3 K, (4) reduced by 1 K, (5) increased by 1 K, (6) increased by 3 K; and (7) a numerical simulation with CMEMS SST data, which varies in time.

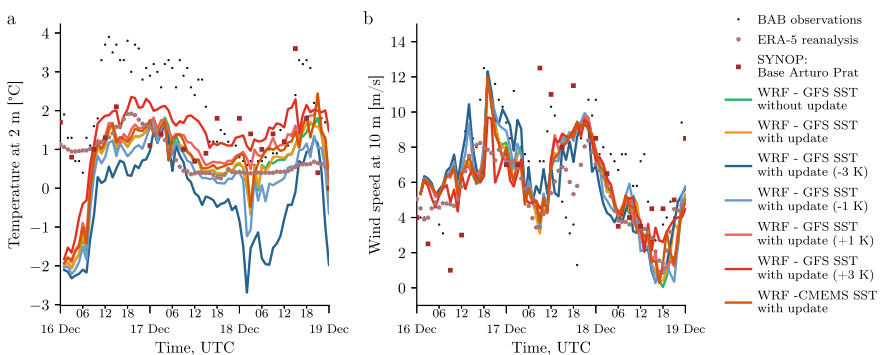
The validation of the 2017 test case shows large discrepancies between the modeled and observed meteorological variables during the cold front passage. In an attempt to improve the numerical forecast and to determine the reasons for these discrepancies, the following simulations are performed: (1) a simulation with a 12-hour spin-up of the model—during the spin-up process, the GFS analysis is used as boundary conditions, not the forecast; (2) a model free run without any update of the boundary conditions after the initialization.

## 4 Assessment of the SST Impact on the Weather Forecast Accuracy

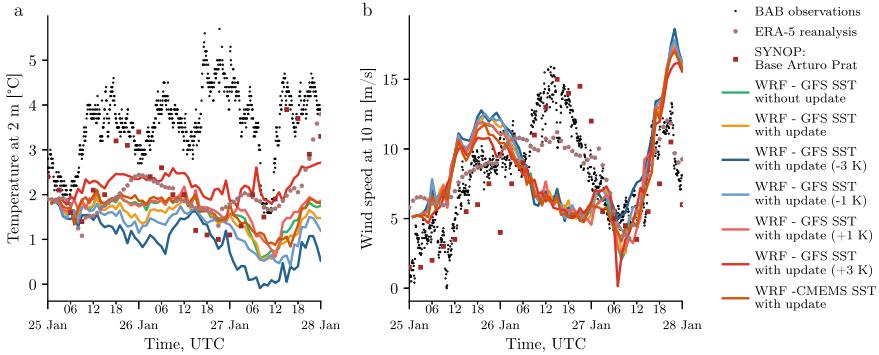
The WRF model validation results demonstrate that the model predicts lower than the observed 2 m temperature. Since the BAB grid point is coastal, it is clear that it will be strongly influenced by the SST. For this reason different experiments are conducted, these include higher GFS SSTs, as well as CMEMS SSTs, which also tend to be higher than the ones by GFS. For symmetry, experiments with lower altered SSTs are also performed. We will first examine the test cases from 2016 and 2020 for which WRF performs well in forecasting the phenomena, associated with the front passage. After this, we will look into the 2017 test case, where a different approach has been applied.

Figure 5 displays the time series of the temperature at 2 m and the wind speed at 10 m according to each SST experiment for the 2016 test case. The graphical comparison shows higher air temperatures values with higher SSTs and accordingly lower air temperatures with lower SSTs, furthermore the lower SSTs result in larger temperature amplitudes. The unmodified curves, corresponding to GFS data with and without time evolving SSTs, are very close, while the CMEMS data result in larger amplitudes. The differences in the 10 m wind speed do not appear to be linear—in the first 36 forecast hours, the highest peaks result from the data with lowest SST, while in the next 36 h the wind speed in this case is the lowest among all simulations.

The forecasts for the 2020 test case, illustrated on Fig. 6, confirm our conclusions for the 2 m temperature, although one can notice a slightly larger distancing between the GFS data forecast curves with and without time evolution. Following the 10 m wind speed curve, the highest peaks are observed with the lowest SSTs, while the minimums are lower with the highest SSTs. The forecast statistics for the 2 m temperature are given in Table 1. In the 2016 and 2020 test cases, the best overall results are



**Fig. 5** A comparison between the temperature at 2 m (a) and wind speed at 10 m (b) between WRF simulations with different SST fields, plotted against BAB measurements (black dots), ERA-5 reanalysis data (brown pentagons) and measurements from a SYNOP station nearby (dark red squares) for the 2016 test case



**Fig. 6** Same as Fig. 5 but for the 2020 test case

**Table 1** Forecast statistics of the temperature at 2 m against measurement data, ERA-5 reanalysis data and the WRF run with unmodified evolving in time SST data from GFS

	BAB measurements			ERA-5 reanalysis			WRF-GFS SST		
	BIAS	RMSE	MAE	BIAS	RMSE	MAE	BIAS	RMSE	MAE
<i>Temperature (°C)</i>									
<i>WRF simulation for the 2016 test case</i>									
WRF-GFS SST without update	-1.45	1.69	1.45	-0.18	0.98	0.62	-0.01	0.07	0.05
WRF-GFS SST with update	-1.44	1.69	1.44	-0.17	0.98	0.62	-	-	-
WRF-GFS SST with update (-3 K)	-2.37	2.47	2.37	-1.11	1.52	1.21	-0.95	1.14	0.95
WRF-GFS SST with update (-1 K)	-1.75	1.93	1.75	-0.48	1.05	0.65	-0.32	0.39	0.32
WRF-GFS SST with update (+1 K)	-1.15	1.51	1.23	0.12	0.99	0.71	0.28	0.34	0.29
WRF-GFS SST with update (+3 K)	-0.70	1.19	0.94	0.58	1.15	1.00	0.75	0.81	0.75
WRF-CMEMS SST with update	-1.30	1.62	1.34	-0.02	0.97	0.66	0.14	0.25	0.20
<i>WRF simulation for the 2017 test case</i>									
WRF-GFS SST without update	-1.11	3.76	3.23	-1.56	3.82	2.75	0.10	0.23	0.13
WRF-GFS SST with update	-1.21	3.86	3.31	-1.67	3.95	2.83	-	-	-
WRF-CMEMS SST with update	-1.33	4.10	3.45	-1.79	4.25	2.98	-0.12	0.61	0.35
WRF—free run	0.39	1.61	1.37	-0.02	1.47	1.18	1.65	3.37	2.62
WRF—with 12-hour spin-up	-1.17	3.84	3.27	-1.42	3.64	2.44	0.03	0.29	0.17
<i>WRF simulation for the 2020 test case</i>									
WRF-GFS SST without update	-1.95	2.11	1.95	-0.38	0.64	0.47	0.12	0.17	0.14
WRF-GFS SST with update	-2.07	2.23	2.07	-0.50	0.75	0.57	-	-	-
WRF-GFS SST with update. (-3 K)	-2.57	2.76	2.57	-1.00	1.25	1.02	-0.50	0.56	0.50
WRF-GFS SST with update (-1 K)	-2.23	2.40	2.23	-0.67	0.90	0.71	-0.16	0.21	0.17
WRF-GFS SST with update (+1 K)	-1.86	2.02	1.86	-0.29	0.57	0.43	0.22	0.26	0.22
WRF-GFS SST with update (+3 K)	-1.32	1.55	1.34	0.25	0.44	0.34	0.75	0.83	0.75
WRF-CMEMS SST with update	-1.89	2.08	1.89	-0.32	0.60	0.44	0.18	0.24	0.20

**Table 2** Forecast statistics of the sea level pressure against measurement data, ERA-5 reanalysis data and the WRF run with unmodified evolving in time SST data from GFS

Pressure (hPa)									
	BAB measurements			ERA-5 reanalysis			WRF-GFS SST		
	BIAS	RMSE	MAE	BIAS	RMSE	MAE	BIAS	RMSE	MAE
<i>WRF simulation for the 2016 test case</i>									
WRF-GFS SST without update	0.58	1.10	0.81	-0.82	1.27	1.14	0.00	0.03	0.02
WRF-GFS SST with update	0.57	1.10	0.81	-0.82	1.27	1.14	-	-	-
WRF-GFS SST with update (-3K)	0.70	1.20	0.88	-0.70	1.22	1.11	0.13	0.17	0.14
WRF-GFS SST with update (-1 K)	0.62	1.13	0.83	-0.78	1.25	1.13	0.05	0.07	0.05
WRF-GFS SST with update (+1 K)	0.53	1.07	0.80	-0.86	1.29	1.15	-0.04	0.06	0.05
WRF-GFS SST with update (+3 K)	0.42	1.01	0.75	-0.98	1.37	1.22	-0.16	0.18	0.16
WRF-CMEMS SST with update	0.55	1.07	0.79	-0.85	1.27	1.14	-0.02	0.05	0.04
<i>WRF simulation for the 2017 test case</i>									
WRF-GFS SST without update	0.74	2.20	1.85	-1.19	2.53	1.71	-0.02	0.04	0.03
WRF-GFS SST with update	0.76	2.21	1.86	-1.16	2.52	1.71	-	-	-
WRF-CMEMS SST with update	0.74	2.21	1.84	-1.19	2.52	1.69	-0.02	0.10	0.08
WRF - free run	0.34	5.49	5.09	-1.60	5.29	4.69	-0.44	5.76	5.26
WRF—with 12-hour spin-up	0.58	2.19	1.86	-1.31	2.48	1.75	-0.17	0.30	0.18
<i>WRF simulation for the 2020 test case</i>									
WRF-GFS SST without update	-0.29	0.73	0.62	-1.39	1.44	1.39	-0.02	0.04	0.03
WRF-GFS SST with update	-0.27	0.72	0.60	-1.37	1.42	1.37	-	-	-
WRF-GFS SST with update. (-3 K)	-0.13	0.69	0.56	-1.23	1.28	1.23	0.14	0.16	0.14
WRF-GFS SST with update (-1 K)	-0.22	0.71	0.58	-1.32	1.37	1.32	0.05	0.06	0.05
WRF-GFS SST with update (+1 K)	-0.33	0.75	0.64	-1.43	1.48	1.43	-0.06	0.08	0.07
WRF-GFS SST with update (+3 K)	-0.57	0.90	0.77	-1.67	1.72	1.67	-0.30	0.33	0.30
WRF-CMEMS SST with update	-0.29	0.73	0.61	-1.39	1.44	1.39	-0.02	0.04	0.03

obtained via the highest (modified) SSTs. Comparing the RMSE of the three unmodified cases with the BAB observations, the CMEMS time-varying SST experiment shows better results than the GFS (time-evolving and non-time-evolving) SST. The forecast statistics calculated against the unmodified WRF run (using GFS SST data without evolution in time) are given in order to distinguish the differences among all simulations. One can spot an almost symmetric linear dependency between the elevated and reduced SST values, as a SST field increase of 3 K results in a 2 m temperature increase at sBAB of 0.75 K.

The sea level pressure statistics, presented in Table 2, differ to a smaller extent. Comparing the modified forecasts, one can notice a decrease in the simulated pressure field, when the SSTs are higher and vice versa.

The differences in the wind speed and direction at 10m between the different simulations are shown in Tables 3 and 4 respectively. With higher SSTs, lower wind speeds are forecast and vice versa. A lowering of the SST field with 3 K may result in a 1 m s<sup>-1</sup> wind speed difference and a deviation in wind direction of almost 30°, according to the model output for the 2016 test case. This may be due to a ratio change

**Table 3** Forecast statistics of the wind speed against measurement data, ERA-5 reanalysis data and the WRF run with unmodified evolving in time SST data from GFS

Wind speed (m/s)									
	BAB measurements			ERA-5 reanalysis			WRF-GFS SST		
	BIAS	RMSE	MAE	BIAS	RMSE	MAE	BIAS	RMSE	MAE
<i>WRF simulation for the 2016 test case</i>									
WRF-GFS SST without update	-0.99	2.69	2.21	0.58	1.48	1.18	-0.03	0.33	0.17
WRF-GFS SST with update	-0.96	2.67	2.18	0.61	1.39	1.10	-	-	-
WRF-GFS SST with update (-3 K)	-0.83	2.67	2.19	0.74	1.69	1.43	0.13	1.13	0.87
WRF-GFS SST with update (-1 K)	-0.90	2.70	2.17	0.67	1.65	1.38	0.06	0.72	0.46
WRF-GFS SST with update (+1 K)	-1.03	2.72	2.20	0.53	1.42	1.12	-0.07	0.57	0.41
WRF-GFS SST with update (+3 K)	-1.03	2.82	2.16	0.53	1.32	1.09	-0.08	1.01	0.75
WRF-CMEMS SST with update	-1.02	2.70	2.21	0.55	1.41	1.09	-0.06	0.56	0.35
<i>WRF simulation for the 2017 test case</i>									
WRF-GFS SST without update	-4.64	8.32	6.49	-1.29	4.56	3.37	0.07	0.45	0.26
WRF-GFS SST with update	-4.70	8.36	6.51	-1.36	4.61	3.36	-	-	-
WRF-CMEMS SST with update	-5.20	8.61	6.62	-1.87	4.84	3.55	-0.51	1.48	0.82
WRF—free run	-0.83	8.32	7.34	2.53	6.23	4.96	3.89	5.45	4.48
WRF—with 12-hour spin-up	-4.67	8.40	6.39	-1.12	4.52	3.19	0.02	1.71	0.93
<i>WRF simulation for the 2020 test case</i>									
WRF-GFS SST without update	-0.06	3.92	3.12	-0.32	3.01	2.51	-0.18	0.43	0.34
WRF-GFS SST with update	0.12	3.95	3.13	-0.14	3.04	2.49	-	-	-
WRF-GFS SST with update. (-3 K)	0.50	4.15	3.33	0.24	3.26	2.73	0.38	0.83	0.60
WRF-GFS SST with update (-1 K)	0.27	4.04	3.18	0.01	3.13	2.55	0.14	0.48	0.35
WRF-GFS SST with update (+1 K)	-0.05	3.99	3.21	-0.31	3.05	2.55	-0.18	0.57	0.41
WRF-GFS SST with update (+3 K)	-0.33	3.81	2.87	-0.59	2.81	2.24	-0.45	1.00	0.75
WRF-CMEMS SST with update	-0.29	3.91	3.02	-0.55	3.01	2.45	-0.41	0.72	0.58

between the surface temperatures of land and sea, which may have induced a breeze-like circulation. The 2020 test case forecast simulations show the same differences in the wind speed field, but the forecasts differ less in wind direction—up to 13°. The lowest RMSE value of the wind speed against ERA-5 data in the 2016 case is observed with the simulation of lowering the SST with 1 K, while for the 2020 case the simulation with best results is the one, where the SST is increased by 1 K.

The 2017 test case is prone to special attention—Fig. 7 shows the 2 m temperature and 10 m wind speed curves. One can see that the WRF forecasts the temperature drop and the wind speed maximum with a delay of about 13 h. Besides, the forecast drop in temperatures reaches lower values than the observed, while the simulated wind speed only reaches values of about 15 m s<sup>-1</sup>, while the observed wind speed goes above 25 m s<sup>-1</sup>. Since no significant improvement is observed via altering the SSTs, two additional simulations are performed - a forecast, preceded by a 12-hour model spin-up and a model free run with the GFS model analysis as an initial condition. The SST in the model is set as time evolving in the spin-up experiment while in the free run it only enters once as an initial condition. The 12-hour spin-up simulation

**Table 4** Forecast statistics of the wind direction against measurement data, ERA-5 reanalysis data and the WRF run with unmodified evolving in time SST data from GFS

Wind direction (deg)	BAB measurements			ERA-5 reanalysis			WRF-GFS SST		
	BIAS	RMSE	MAE	BIAS	RMSE	MAE	BIAS	RMSE	MAE
<i>WRF simulation for the 2016 test case</i>									
WRF-GFS SST without update	-5.52	33.46	26.59	-1.09	36.99	27.28	2.50	20.68	6.47
WRF-GFS SST with update	-6.15	35.14	27.48	-3.60	35.61	26.76	-	-	-
WRF-GFS SST with update (-3 K)	-12.18	40.53	30.48	-4.02	37.14	26.40	-0.42	27.33	13.64
WRF-GFS SST with update (-1 K)	-7.84	37.32	29.97	2.76	34.70	26.07	6.36	28.81	10.63
WRF-GFS SST with update (+1 K)	-4.76	32.40	25.09	-1.80	42.15	28.81	1.80	19.07	8.37
WRF-GFS SST with update (+3 K)	-13.19	41.77	35.35	-11.24	38.74	29.34	-2.64	23.87	12.47
WRF-CMEMS SST with update	-5.62	32.83	26.47	-3.66	41.79	28.51	-0.06	15.13	6.97
<i>WRF simulation for the 2017 test case</i>									
WRF-GFS SST without update	-33.01	119.28	110.08	-53.35	100.91	83.71	-0.29	3.97	2.05
WRF-GFS SST with update	-32.18	119.22	109.55	-53.07	99.88	83.46	-	-	-
WRF-CMEMS SST with update	-35.53	121.54	112.31	-54.79	106.24	89.83	-6.72	23.34	9.66
WRF-free run	10.01	52.28	47.07	29.76	78.64	52.42	22.83	70.09	55.23
WRF-with 12-hour spin-up	-33.43	121.45	112.40	-44.52	97.48	78.21	-4.38	18.36	7.84
<i>WRF simulation for the 2020 test case</i>									
WRF-GFS SST without update	-53.41	58.77	54.14	-16.14	26.80	20.97	-0.51	3.43	1.91
WRF-GFS SST with update	-52.90	58.27	53.68	-15.63	26.76	21.16	-	-	-
WRF-GFS SST with update. (-3 K)	-55.95	61.67	56.34	-18.68	30.42	23.16	-3.04	6.37	4.33
WRF-GFS SST with update (-1 K)	-53.78	59.03	54.33	-16.51	27.39	21.78	-0.88	3.74	2.39
WRF-GFS SST with update (+1 K)	-53.11	58.10	53.57	-15.84	25.95	21.11	-0.21	6.87	3.58
WRF-GFS SST with update (+3 K)	-52.13	58.41	52.63	-14.85	26.15	20.62	0.78	12.75	6.44
WRF-CMEMS SST with update	-54.31	59.25	54.73	-17.04	26.77	21.10	-1.40	4.59	2.97

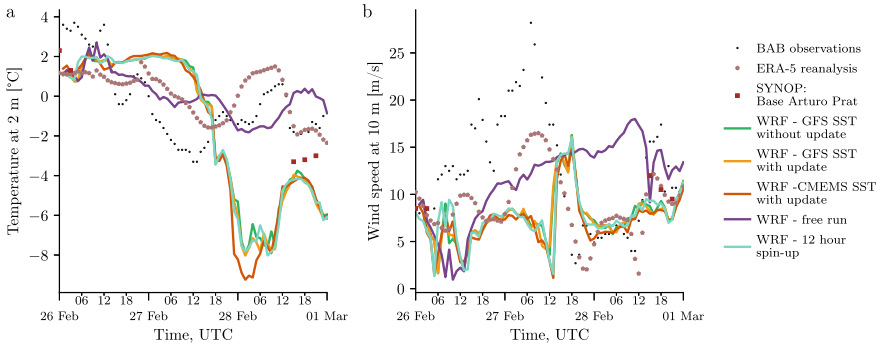


**Fig. 7** Same as Fig. 5 but for the 2017 test case

is similar to the original forecasts and performs better in the initial forecast hours, when it shows higher temperatures and higher wind speeds. The ranges of the 2 m temperature, simulated in the free run, are closer to the observed ones, but the forecast curve moves behind the events. The free run simulation does not perform well in forecasting the wind speed at 10 m. The earlier illustrated sudden temperature drop in CMEMS SSTs (Fig. 3) only deepens the temperature minimum and this results in a higher RMSE value, compared to the other simulations in Table 1. According to the forecast statistics for the 2017 test case in Table 2, the sea level pressure is best forecasted in the 12-hour spin-up simulation, which pinpoints the negative impact of the coarse initial condition on high resolution numerical models. The necessity of lateral boundary conditions is demonstrated by the large differences in sea level pressure, simulated in the model free run.

The comparison between the wind speed and direction in the 2017 test case against ERA-5 data shows best results in the 12-hour spin-up simulation. The forecast statistics for the wind directions are most promising in the free run with RMSE values more than 2 times lower than in the other simulations. This may imply that the wind field around BAB is influenced by some local circulation and the boundary conditions, incoming from the GFS, worsen the forecast in the 2017 test case.

## 5 Relation Between the Meteorological Variables and the Modification of SST

The symmetrical planning of our numerical experiments for the 2016 and 2020 test cases enables us to construct the dependencies of some of the meteorological variables against the applied modification of SST. This approach deals entirely with model data, and thus the analysis cannot be affected by observational errors. In order to quantify the SST field modification, let us introduce the variable  $\Delta SST$ , which only takes discrete values of  $-3$ ,  $-1$ ,  $0$ ,  $1$  and  $3$  K. These values correspond to the five simulations, in which the SST has been equally modified in each sea point of the model grid. When  $\Delta SST = 0$ , the SST field consists of the unmodified values, provided by the GFS model. In this section, we will only consider the temperature at 2 m, sea level pressure and wind speed at 10 m in the 24th forecast hour in the finest domain—d03. This hour has been chosen to be sufficiently ahead in time for the forecasted field not to be disturbed by the initial condition, and to properly represent the model characteristics. For the 2016 test case the 24th forecast hour corresponds to 17.12.2020 0 UTC, and for the test case in 2020 this is 26.01.2020 0 UTC. Let us introduce the variables  $T_{min}$ ,  $P_{min}$  and  $V_{min}$ , which represent the minimum value of the whole model domain d03 in the 24th hour of the variables 2 m temperature, sea level pressure and 10 m wind speed respectively. In the same way, we can introduce  $T_{max}$ ,  $P_{max}$  and  $V_{max}$  as the corresponding maximums in the field at that moment. The aggregate of all field values will be represented by the aerial average values  $\bar{T}$ ,

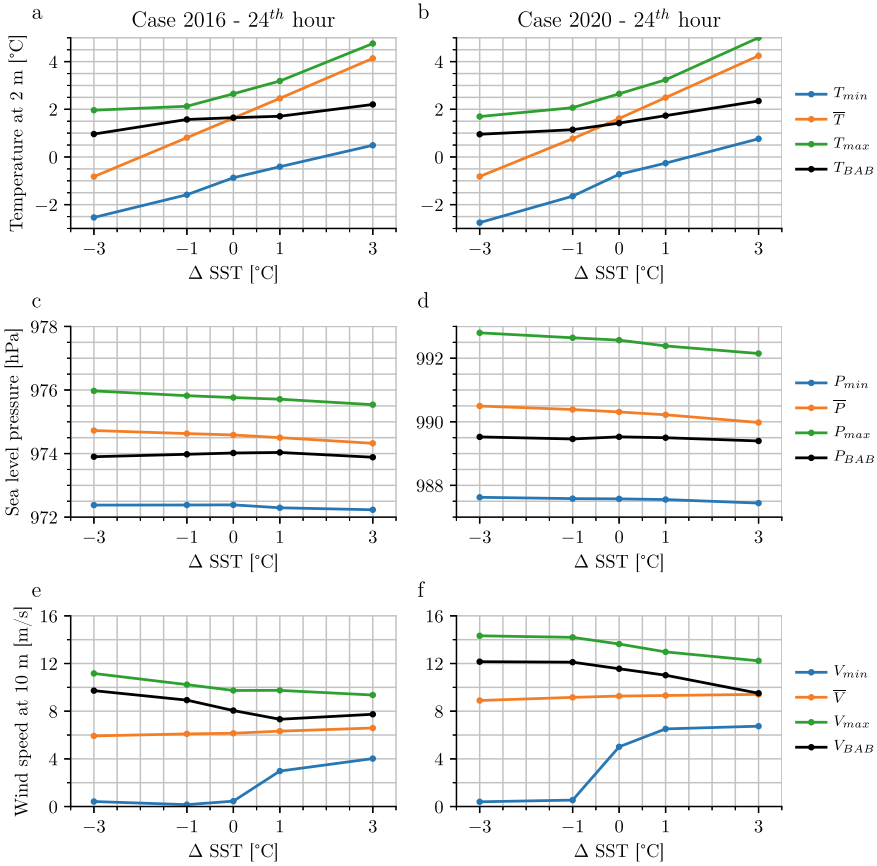


**Fig. 8** Relations between  $\Delta \text{SST}$  and the field characteristics of T, P and V for the 24th forecast hour for the 2016 test case (left column) and the 2020 test case (right column)

$\bar{P}$  and  $\bar{V}$ . The values at the BAB point at the 24th forecast hour will be denoted as  $T_{BAB}$ ,  $P_{BAB}$  and  $V_{BAB}$ .

Figure 8 presents the relations between the different field characteristics and the imposed modification of SST for the 2016 and 2020 test cases. As anticipated, the 2m temperature increases when we rise the SST, as  $T_{min}$  rises more steeply than  $T_{max}$ . The temperature value at BAB  $T_{BAB}$  is the least affected by the numerical modification, because it characterizes only the temperature over land, while the other characteristics are representative for the whole domain, which is mostly composed of sea grid points. Consequently, a change in the SST has a greater impact on the 2m temperature over water than over land.

Looking through the change in the sea level pressure characteristics, given in Fig. 8c and d, one can see that an increase in SST leads to lower pressure values in both test cases. The value of  $P_{max}$  is reduced more by the increase compared to  $P_{min}$ .

The fact the curves  $\bar{P}$  and  $P_{BAB}$  have similar behavior illustrates that the sea level pressure field is homogeneously affected throughout the model domain.

The 10 m wind speed characteristics, given in Fig. 8e and f, show a non-linear increase of  $V_{min}$ . This sudden “jump” suggests that there is a value of  $V$ , above which additional processes are unlocked, which significantly increase the wind speed at the points of null speed. The decrease in  $V_{max}$  and  $V_{BAB}$ , but increase in  $\bar{V}$  shows that the wind speed is differently affected in different grid points. However, its average value slightly increases with rising SST.

The conducted sensitivity experiments show that all of the considered meteorological variables are affected by the sea surface temperature, the most prominent differences being observed in the 2 m temperature field. With an uniform rise in SST, the corresponding tendencies are: an increase of the 2 m temperature, a decrease of the sea level pressure and an increase of the average wind speed. For the BAB region, the best results with unmodified data are obtained when using SST data from the CMEMS operational ocean model [5].

## 6 Conclusion and Outlook

The performed numerical experiments show that the results are rather influenced by the choice of the SST field as initial and boundary conditions for the weather forecast at the Bulgarian Antarctic base area. The examination of the time evolution of the different SST fields coming from the operational global models GFS and CMEMS indicates that the SST field is difficult to forecast and may vary rapidly of more than 2.5 K in the range of 48 h. Based on the model validation and the availability of modeled and measured water temperature data in the BAB bay, different experiments with different SSTs have been planned. The conducted experiments with the regional WRF show that increasing the SST leads to a rise in the 2 m temperature in the whole model grid, while the sea level pressure decreases linearly. The relationship between wind speed at 10 m and SST is more complex - with increasing the SST, the maximum wind speed decreases and the minimum suffers a non-linear increase.

The different numerical experiments in the BAB region show that an increase of SST with 3 K leads to an increase of the 2 m temperature at BAB with 0.75 K, which reduces the RMSE. Overall, the numerical model underestimates the temperature, which is supposedly due to an inappropriate representation of the land surface cover. In order to increase the forecast skill in the summer season, a revision of the land use type is advisory. The simulations with model spin-up show slightly improved results. Optimum results with unmodified data are obtained, when using evolving in time CMEMS SST as model input. The authors recommend regular in situ measurements of the SST in the BAB bay, which will allow to calculate the global forecast SST bias in the area. The BAB modelling system configuration is modified to use the CMEMS global ocean forecast analysis and forecast as surface boundary condition in operational mode.

## References

1. Bai, H., Hu, H., Yang, X.Q., Ren, X., Xu, H., Liu, G.: Modeled MABL responses to the winter Kuroshio SST front in the East China Sea and Yellow Sea. *J. Geophys. Res.: Atmos.* **124**(12), 6069–6092 (2019). <https://agupubs.onlinelibrary.wiley.com/doi/abs/10.1029/2018JD029570>
2. Chtirkova, B.: A study on the impact of sea surface temperature on the weather forecast for the Bulgarian Antarctic base on Livingston Island. Master's thesis (2020)
3. Chtirkova, B., Peneva, E.: The impact of SST on the weather forecast quality in the Bulgarian Antarctic Base area on Livingstone Island (2020). <https://doi.org/10.5194/egusphere-egu2020-9347>
4. Chtirkova, B., Peneva, E., Georgieva, G.: A modelling system for numerical weather prediction in the Bulgarian Antarctic Base area. In: Proceedings of the 1st International Conference on Environmental Protection and Disaster Risks, 29 Sept–1 Oct 2020, Sofia, Bulgaria (2020)
5. Copernicus: Copernicus Marine Environment Monitoring Service (2020). <https://marine.copernicus.eu/>
6. Hersbach, H., Bell, B., Berrisford, P., Hirahara, S., Horányi, A., Muñoz-Sabater, J., Nicolas, J., Peubey, C., Radu, R., Schepers, D., Simmons, A., Soci, C., Abdalla, S., Abellan, X., Balsamo, G., Bechtold, P., Biavati, G., Bidlot, J., Bonavita, M., Chiara, G., Dahlgren, P., Dee, D., Diamantakis, M., Dragani, R., Flemming, J., Forbes, R., Fuentes, M., Geer, A., Haimberger, L., Healy, S., Hogan, R.J., Hólm, E., Janisková, M., Keeley, S., Laloyaux, P., Lopez, P., Lupu, C., Radnoti, G., Rosnay, P., Rozum, I., Vamborg, F., Villaume, S., Thépaut, J.N.: The ERA5 global reanalysis. *Q. J. R. Meteorol. Soc.* **146**(730), 1999–2049 (2020). <https://doi.org/10.1002/qj.3803>
7. Ivanov, L.L.: Antarctica: Livingston Island and Smith Island. Scale 1:100000 topographic map. Manfred Wörner Foundation (2017)
8. Miglietta, M.M., Moscatello, A., Conte, D., Mannarini, G., Lacorata, G., Rotunno, R.: Numerical analysis of a Mediterranean ‘hurricane’ over south-eastern Italy: sensitivity experiments to sea surface temperature. *Atmos. Res.* **101**(1–2), 412–426 (2011). <https://doi.org/10.1016/j.atmosres.2011.04.006>
9. NCAR/UCAR: The Antarctic Mesoscale Prediction System (AMPS) (2020). <https://www2.mmm.ucar.edu/rt/amps/>
10. Senatore, A., Mendicino, G., Knoche, H.R., Kunstmann, H.: Sensitivity of modeled precipitation to sea surface temperature in regions with complex topography and coastlines: a case study for the mediterranean. *J. Hydrometeorol.* **15**(6), 2370–2396 (2014). <https://doi.org/10.1175/JHM-D-13-089.1>
11. Skamarock, W.C., Klemp, J.B., Dudhia, J., Gill, D.O., Liu, Z., Berner, J., Wang, W., Powers, J.G., Duda, M.G., Barker, D.M., Huang, X.Y.: A description of the advanced research WRF model version 4. UCAR/NCAR (2019). 10.5065/1DFH-6P97. <https://opensky.ucar.edu/islandora/object/opensky:2898>
12. Tuleya, R.E., Kurihara, Y.: A note on the sea surface temperature sensitivity of a numerical model of tropical storm genesis. *Mon. Weather Rev.* **110**(12), 2063–2069 (1982). [https://doi.org/10.1175/1520-0493\(1982\)1102063:ANOTSS2.0.CO;2](https://doi.org/10.1175/1520-0493(1982)1102063:ANOTSS2.0.CO;2)